

Antiferromagnetic-to-ferrimagnetic phase transition with large electric-polarization change in a frustrated polar magnet $\text{CaBaCo}_4\text{O}_7$

Tsuyoshi Omi,¹ Yoshito Watanabe,¹ Nobuyuki Abe,¹ Hajime Sagayama,² Akiko Nakao,³ Koji Munakata,³ Yusuke Tokunaga,¹ and Taka-hisa Arima¹

¹Department of Advanced Materials Science, The University of Tokyo, 277-8561 Kashiwa, Japan

²Institute of Materials Structure Science, High Energy Accelerator Research Organization, 305-0801 Tsukuba, Japan

³Comprehensive Research Organization for Science and Society, 319-1106 Tokai, Japan



(Received 6 February 2020; revised 10 December 2020; accepted 29 April 2021; published 12 May 2021)

We investigate phase transitions of a geometrically frustrated polar magnet $\text{CaBaCo}_4\text{O}_7$, which exhibits the largest magnetoelectric (ME) effect in multiferroic compounds reported so far. Measurements of magnetization, sound velocity, and neutron diffraction of single crystals reveal an antiferromagnetic phase between the ferrimagnetic transition temperature $T_C \sim 60$ K and $T^* \sim 69$ K. In the antiferromagnetic phase, the ordered Co moments on the triangular layers remain nearly disordered. We demonstrate that a large electric-polarization change emerges upon the antiferromagnetic-to-ferrimagnetic transition. The large ME coupling can be attributed to the exchange striction.

DOI: [10.1103/PhysRevB.103.184412](https://doi.org/10.1103/PhysRevB.103.184412)

I. INTRODUCTION

Magnetoelectric (ME) coupling in multiferroic materials, where particular electric and magnetic orders coexist, is expected to bring us benefits for the technological application to energy-saving memory devices and sensors [1,2]. Since the first observation of an ME effect in Cr_2O_3 [3], the scientific interest in enhancing ME coupling has deepened the understanding of the origin of ME coupling [4]. Manipulating magnetic frustration is a key to enhancing ME coupling. Particular magnetic structures such as the spin cycloid, which often emerges in systems with degenerate low-energy states due to magnetic frustration, induce electric polarization. Triggered by the report of magnetic control of ferroelectric polarization and gigantic ME coupling in the frustrated spiral magnet TbMnO_3 [5], the ME effect has been extensively explored in frustrated multiferroics such as the zigzag chain antiferromagnet MnWO_4 [6,7], the kagome-staircase antiferromagnet $\text{Ni}_3\text{V}_2\text{O}_8$ [8], and the triangular antiferromagnetic delafossite CuFeO_2 [9–11].

The Swedenborgite $\text{CaBaCo}_4\text{O}_7$ is a pyroelectric which belongs to the polar orthorhombic space group $Pbn2_1$. Triangular and kagome layers formed by Co ions alternately stack along the polar c axis. Qu *et al.* suggested strong magnetic frustration in the Co network [12]. Magnetic moments of Co^{2+} and Co^{3+} exhibit noncollinear ferrimagnetic order below $T_C \sim 60$ K with the easy axis along the b axis [13]. At the ferrimagnetic transition, $\text{CaBaCo}_4\text{O}_7$ shows a large change, ΔP , in electric polarization of about 17 mC/m^2 [14], which is one or two orders larger than that of the above-mentioned multiferroics. In addition to the large ΔP , an anomaly is observed in the c -axis length at T_C [15]. An electric-polarization change of about $\Delta P \sim 8 \text{ mC/m}^2$ is also induced by a magnetic field at a temperature right above T_C . In regard to the large ME coupling, a large magnetocapacitance effect [16] and unidirectional terahertz light absorption [17] were recently reported.

Such a large ME response across the ferrimagnetic transition may be explained by exchange striction [18,19]. Nonetheless, the nature of the state just above T_C in zero magnetic field is still controversial. Some physical measurements propose the presence of another phase transition at $T^* \sim 69$ K, which is considerably higher than T_C . Caignaert *et al.* inferred that the anomaly should not be of magnetic origin by measuring electric permittivity and specific heat [14], while Yu *et al.* pointed out that it should be caused by lower-frequency dynamics associated with critical fluctuations near T_C or the dynamics of magnetic domains [20]. The temperature dependence of magnetization of related compounds where Co ions in $\text{CaBaCo}_4\text{O}_7$ are partially replaced by other magnetic or nonmagnetic ions shows an anomaly presumed to be concerned with the anomaly at T^* in pure $\text{CaBaCo}_4\text{O}_7$ [21,22]. Based on the result of powder neutron diffraction, Seikh *et al.* have concluded that the anomaly in $\text{CaBaCo}_{3.97}\text{Zn}_{0.03}\text{O}_7$ corresponds to the magnetic transition from paramagnetic to incommensurate helical or spiral magnetic structure [23]. Lohr *et al.* have pointed out a modulated spin structure with the propagation vector $\mathbf{k} = (1/2, 1/2, 0.02)$ in $\text{Ca}_{0.98}\text{Sr}_{0.02}\text{BaCo}_4\text{O}_7$ [24]. Identification of the intermediate-temperature phase between T_C and T^* is necessary to clarify the nature of the gigantic ME response in $\text{CaBaCo}_4\text{O}_7$, which will bring about a beneficial guideline in the search for multiferroic materials with strong ME coupling. Here, we report on the temperature dependence of electric permittivity, ultrasound velocity, and magnetization of $\text{CaBaCo}_4\text{O}_7$. A single-crystal neutron diffraction measurement clearly shows antiferromagnetic order with cell doubling in the intermediate-temperature phase.

II. METHODS

Single crystals of $\text{CaBaCo}_4\text{O}_7$ were grown by a floating-zone method [16]. A stoichiometric mixture of powders of

CaCO₃, BaCO₃, and Co₃O₄ was first heated at 900 °C in air for 12 h. The resulting powders were pressed into a rod, sintered at 1100 °C for 12 h in air [25], and quenched down to room temperature. The crystal growth was performed by using a floating-zone furnace. The melting zone was transferred in air at a rate of 1 mm/h. At the end of the growth, the crystal rod was quenched down to room temperature. Single-phase CaBaCo₄O₇ was obtained near the top of the rod (i.e., end point of the growth). Temperature T dependence of magnetization M was measured by using a magnetometer (MPMS, Quantum Design). Electric polarization P was calculated by the integration of the displacement current obtained by using an electrometer (6517A, Keithley). The dielectric constant ϵ_c along the polar c axis was measured at 103 kHz by using an inductance-capacitance-resistance (LCR) meter (E4980A, Keysight Technologies). The T dependence of P and ϵ_c was collected by using a commercial measurement system (PPMS, Quantum Design). Ultrasound velocity measurements were performed by the pulse-echo method [26] using an 8-T superconducting magnet. A pair of LiNbO₃ piezoelectric transducers were attached on opposite surfaces of a single crystal. Longitudinal transducers were used to measure the change in the relative velocity (dv/v) of the first echo in the configuration that the ultrasonic propagation vector \mathbf{k} was perpendicular to the c axis. Neutron diffraction experiments were carried out using a time-of-flight Laue single-crystal neutron diffractometer, SENJU [27] on BL-18 at the Materials and Life Science Experimental Facility of the Japan Proton Accelerator Research Complex. The wavelength range of incident neutrons was selected to be between 0.4 and 4.4 Å using bandwidth choppers. A crystal of dimensions of about $2 \times 3 \times 4$ mm³ glued to an aluminum bar was mounted on a goniometer. The crystal was twinned due to the trigonal-orthorhombic structure transition above room temperature [28,29]. The neutron diffraction pattern was measured with a step of 1 K while warming from 58 to 78 K. The Lorentz factor, the pixel sensitivity, the resolution, and the spectrum of the incident neutrons were corrected by using the software STARGAZER [27]. The intensities shown in this paper are integrated intensities after such corrections. The magnetic structure was analyzed by minimizing the sum of the square of the residual between observed magnetic Bragg intensities after the correction mentioned above and calculated intensities. Crystal and magnetic structures were visualized by VESTA software [30].

III. RESULTS

Figure 1(a) shows the T dependence of M in a magnetic field $H = 100$ Oe perpendicular to the c axis. M shows steep changes at 62 K on warming and 61 K on cooling. The anomalies correspond to a first-order ferrimagnetic transition, as previously reported [13,14,29]. The electric-polarization change ΔP_c and ϵ_c measured along the polar c axis at $H = 0$ are shown in Fig. 1(b). At T_C , ΔP_c suddenly changes by about 5 mC/m², and ϵ_c shows a peak, suggesting the strong magnetoelectric coupling in CaBaCo₄O₇ [16]. The velocity of longitudinal sound propagating in the c plane also exhibits an anomaly at T_C , as shown in Fig. 1(c). We consider that the softening of the elastic constant should be related to the change in the lattice parameters at T_C [15].

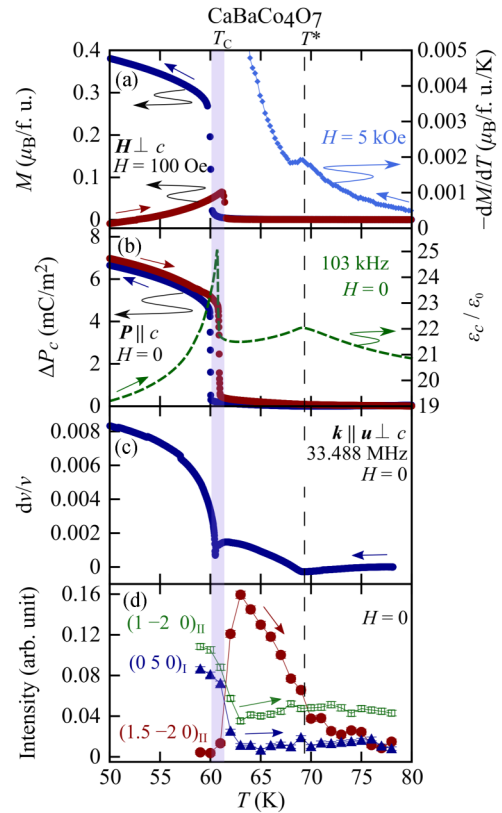


FIG. 1. (a) Temperature dependence of magnetization M perpendicular to the c axis in $H = 100$ Oe and its temperature derivative $-dM/dT$. Blue and red dots represent M measured upon cooling and upon warming after zero-field cooling, respectively. (b) Change in electric polarization ΔP_c with temperature (blue and red dots) and electric permittivity ϵ_c at 103 kHz (dashed line) along the c axis. (c) Temperature dependence of longitudinal ultrasound velocity v propagating perpendicular to the c axis. (d) Temperature dependence of integrated intensities of neutron reflections at $(1.5 - 2.0)$ (circles), $(0.5 0)$ (triangles), and $(1 - 2.0)$ (rectangles). The indices of $(1.5 - 2.0)$ and $(1 - 2.0)$ are equivalent to those of $(1.75 1.25 0)$ and $(1.5 0.5 0)$ of domain I shown in Fig. 2(b), respectively. Here, the background intensities are subtracted. The vertical stripe and the dashed line denote the ferrimagnetic transition temperature T_C with a hysteresis and the antiferromagnetic transition temperature T^* , respectively.

In addition to the ferrimagnetic transition, a small peak appears in ϵ_c at $T^* = 69$ K, as reported in Ref. [14]. Moreover, we find anomalies in M and dv/v as well as at T^* . The T derivative of the magnetization exhibits a cusp at T^* , as shown in Fig. 1(a). These anomalies in physical properties indicate the existence of another phase transition at T^* .

In order to identify the magnetic state of CaBaCo₄O₇ between T_C and T^* , a neutron diffraction measurement is conducted. The T dependence of the intensities of several reflections is shown in Fig. 1(d). Here, the Miller indices are based on one of three kinds of orthorhombic domains. The intensity of the $(1.5 - 2.0)$ reflection increases with decreasing temperature from T^* to T_C and then suddenly disappears at T_C , as shown in Fig. 1(d). The presence of $(m + 1/2 k 0)$ peaks with integers m and k indicates the doubling of the

magnetic unit cell along the a axis in this temperature range.

In contrast to the $(1.5-2\ 0)$ reflection, the intensity of the $(0\ 5\ 0)$ reflection is nearly zero above T_C and increases below T_C . It is of note here that the $(0\ 5\ 0)$ reflection is forbidden for the space group $Pbn2_1$. The increase in the scattering intensity below T_C is explained by the ferrimagnetic order proposed in Ref. [13]. The $(1.5\ 0.5\ 0)$ reflection, which is equivalent to $(1-2\ 0)$, is also explained by considering the ferrimagnetic order and the presence of the crystallographic twins, as is discussed in more detail later.

Next, we study the T dependence of the neutron diffraction pattern on the $(h\ k\ 0)$ plane in detail. In the paramagnetic phase, nuclear reflections appear on the lattice points in the reciprocal space, as shown in Fig. 2(d). Diffraction peaks are also observed at $(h\ k\ 0)$ with both h and k being half integers, such as $(2.5\ 1.5\ 0)$. They should be attributed to twinned domains. $\text{CaBaCo}_4\text{O}_7$ undergoes a trigonal-to-orthorhombic structural phase transition with a common c axis due to buckling of the CoO_4 tetrahedra on the kagome layers [28,29]. Figures 2(a) and 2(b) show arrangements of Co ions in the trigonal and orthorhombic phases, respectively. Twinned domains with three different b -axis orientations are formed reflecting the high-temperature trigonal structure, as shown in Fig. 2(c) [19]. We take the twinned domains into account to analyze neutron diffraction patterns. Arrows in Fig. 2(d) denote directions of the a^* and b^* axes for three crystallographic domains with different orientations. The $(h\ k\ l)$ reflection of the domains rotated by $\pm 60^\circ$ about the c axis appears at around $((h \mp k)/2\ (\pm 3h + k)/2\ l)$.

Now we focus on the diffraction pattern at 65 K [Fig. 2(e)] considering the multidomains. Some reflections which are not seen in the paramagnetic phase appear in the intermediate-temperature phase, such as $(1.5\ 0\ 0)$ and $(-1.25\ 3.75\ 0)$, as shown in Fig. 2(e). Such superlattice reflections are clearly observed only in the low- q range. In addition, they are not observed in x-ray diffraction (not shown here). These two features suggest that superlattice reflections should be caused by magnetic order.

The superlattice reflections at 65 K can be indexed as $(m + 0.5, n, l)$ and $(m \pm 0.25, n \pm 0.25, l)$ (m, n, l : integers). No reflections are observed for noninteger l 's. A single propagation vector of $(1/2, 0, 0)$ can explain the diffraction pattern by considering the twins. $(m \pm 0.25, n \pm 0.25, l)$ reflections can be obtained by rotating $(m' + 0.5, n', l)$ reflections by $\pm 60^\circ$. For example, $(1.75 \pm 1.25\ 0)$ reflections can be explained by rotating the $(1.5\ 0\ 0)$ reflection by $\pm 60^\circ$. We also observe weak reflections at some $(m, n + 0.5, l)$ positions. They can be ascribed to double scattering of neutrons composed of nuclear reflections in domains II or III and magnetic reflection in domain I. Although we cannot completely exclude the possible modulation along the b axis, it must be minor even if it exists. We also note that the position of the $(2\ 0.5\ 0)$ reflection is shifted from the center of $(2\ 0\ 0)$ and $(2\ 1\ 0)$. The ratio of a^* to b^* in $\text{CaBaCo}_4\text{O}_7$ is a little larger than $\sqrt{3}$ [15]. Therefore the peak positions for the different orthorhombic twin domains do not form a regular lattice. The shift of the position of the reflection around $(2\ 0.5\ 0)$ implies that the peak does not arise from domain I, which may support our interpretation that the b axis should not be doubled in the

antiferromagnetic phase. Instead, we assign the peak around $(2\ 0.5\ 0)$ to the double scattering; a fundamental reflection of domain II or III at around $(h + 1/2, k + 1/2, l)$ and a magnetic peak of domain I at $(-h + 1 + 1/2, -k, -l)$. We conclude that magnetic order which doubles the unit cell along the a axis emerges in the intermediate-temperature phase.

Compared with the diffraction pattern in the paramagnetic phase, additional reflections such as $(0\ 5\ 0)$ and $(2.5\ 2.5\ 0)$ emerge in the low-temperature ferrimagnetic phase [Fig. 2(f)]. Note that $(0\ k\ 0)$ reflections with odd k are forbidden by the b -glide symmetry in the paramagnetic phase but satisfy the reflection condition by the ferrimagnetic spin arrangement proposed in Ref. [13]. In fact, there appear peaks at $(0\ 5\ 0)$ and $(2.5\ 2.5\ 0)$, corresponding to $(0\ -5\ 0)$ in domain III, in the ferrimagnetic phase.

A simple description of the resultant nuclear peak positions for the paramagnetic phase and additional magnetic ones for antiferromagnetic and ferrimagnetic phases in the absence of orthorhombic twin domains is schematically shown in Figs. 2(g), 2(h), and 2(i), respectively.

IV. DISCUSSION

Here, we discuss the magnetic structure in the intermediate-temperature phase. Magnetization in this phase is much smaller than that in the ferrimagnetic phase. The absence of spontaneous magnetization has also been reported in the literature [14]. Based on the present magnetization and neutron diffraction data, we assume the existence of the symmetry operation of the combination of the time reversal and the translation by \mathbf{a} .

The magnetic structure is analyzed by least-squares fitting (Table I). Intensities of 34 magnetic reflections (in condition $I_{\text{obs}} > 3\sigma$ and $I_{\text{obs}} > 2I_{\text{BG}}$, where I_{BG} is background intensity) are collected at $T = 65$ K. The n -glide plane perpendicular to the b axis is broken with the cell doubling along the a axis. Considering the crystallographic space group $Pbn2_1$, possible magnetic symmetries are monoclinic $P_{2a}b11$ or $P_{2a}112_1$ or lower triclinic symmetries with the time-reversal translation symmetry. We fit the data by optimizing the magnetic moments of eight independent Co ions as well as the domain ratio of twins with three different b -axis orientations for two magnetic models with monoclinic structures [32]. Residual factors are $R = 12.7\%$ for $P_{2a}b11$ and $R = 10.0\%$ [$\omega R = 14.0\%$, goodness of fit (GOF) = 2.66] for $P_{2a}112_1$. A favorable model to describe the magnetic structure in the intermediate-temperature phase is $P_{2a}112_1$, as shown in Fig. 3(c). The antiferromagnetic phase appears in a narrow temperature range just below the magnetic transition temperature. The ordered moments do not sufficiently grow in the phase, and the statistics of magnetic reflections were rather low. The intensity of each magnetic reflection was further reduced by the presence of three domains. We hence obtained the domain ratio by analyzing the fundamental Bragg reflections and used all the magnetic reflections for analyzing the magnetic structure. Although we also analyzed the data for only one orthorhombic domain, the reliability was higher when we used all the magnetic reflections.

Figures 3(a) and 3(b) show the magnetic structures projected onto the c plane in the intermediate- and

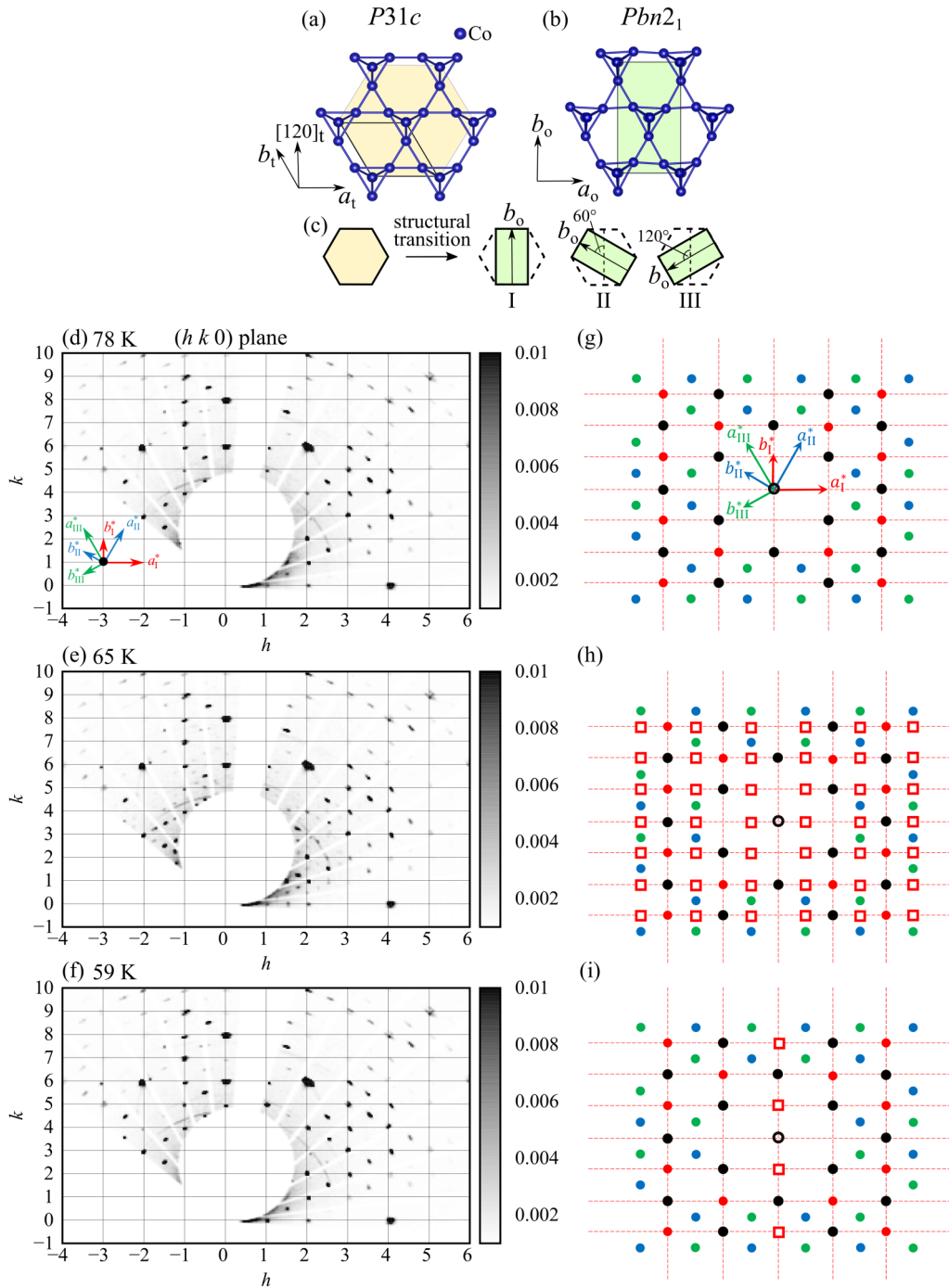


FIG. 2. (a) and (b) Arrangement of Co ions projected onto the c plane in the (a) trigonal ($P31c$ [28]) and (b) orthorhombic ($Pbn2_1$) phases of $\text{CaBaCo}_4\text{O}_7$. Thin black lines show unit cells. (c) Schematic illustration of the trigonal-to-orthorhombic transformation. a_t and b_t (a_o and b_o) denote crystal axes in the trigonal (orthorhombic) system. Three states with different b_o -axis orientations may exist [31]. (d)–(f) Temperature dependence of neutron diffraction patterns in the $(h k 0)$ plane at (d) 78 K, (e) 65 K, and (f) 59 K. Radial white slit regions are not measured because of the absence of the detector. Arrows in (d) denote the directions of the a^* and b^* axes for three crystallographic domains with different axis orientations. Note that domains II and III produce nuclear reflections at $(m + 0.5, n + 0.5, l)$ (m, n, l : integers). (g)–(i) Schematics of the positions of nuclear reflections (circles) and magnetic reflections (squares) in (g) paramagnetic, (h) antiferromagnetic, and (i) ferrimagnetic phases for the orthorhombic phase on the reciprocal $(h k 0)$ plane.

low-temperature phases, respectively. The ordered moment of Co1 on the triangular layer is smaller than those of Co ions on the kagome layer in the intermediate-temperature antiferromagnetic phase. The magnetic moments on the triangular layer are arranged essentially below T_C . A similar partially

ordered state emerges in the intermediate-temperature phase in GeNi_2O_4 , which also has alternate stacking of triangular and kagome layers formed by magnetic ions [33,34]. The magnetic structure in the intermediate-temperature phase comprises two kinds of columns, A and B, as shown in

TABLE I. Magnetic parameters for $\text{CaBaCo}_4\text{O}_7$ at 65 K. Only the moments in an independent quadrant ($0 < x < 1$, $0 < z < 1/2$) are listed. The magnetic space group is $P_{2a}112_1$. There exist two kinds of Co columns [see Fig. 3(a)], columns A and B. Note that columns A and B are on 2_1 and $2'_1$ axes, respectively.

Site	m_a (μ_B)	m_b (μ_B)	m_c (μ_B)	$ m $ (μ_B)
A Co1(T)	-0.01(4)	-0.05(3)	-0.05(2)	0.07(2)
B Co1(T)	0.06(2)	0.09(3)	-0.01(1)	0.11(2)
A Co2(K)	-0.02(1)	0.09(2)	0.05(3)	0.11(2)
B Co2(K)	0.12(5)	0.09(4)	0.00(1)	0.15(5)
A Co3(K)	-0.17(2)	0.01(2)	0.07(2)	0.19(2)
B Co3(K)	0.27(3)	0.14(2)	-0.06(4)	0.32(3)
A Co4(K)	-0.23(2)	0.01(2)	0.00(2)	0.23(2)
B Co4(K)	0.21(3)	-0.21(2)	0.17(3)	0.34(2)

Fig. 3(a). Column A is on a 2_1 screw axis, while column B is on a $2'_1$ time-reversal screw axis. As a result, the in-plane components on kagome layers stack antiferromagnetically and ferromagnetically in columns A and B, respectively. The net magnetizations are canceled out due to the cell doubling. In the ferrimagnetic phase, magnetic moments on triangular layers and those on kagome layers are ferrimagnetically arranged with the easy axis along the b axis, as shown in Fig. 3(b) [13]. The observed two-step magnetic transitions are rather extraordinary. It would be interesting to study the microscopic origin of the antiferromagnetic-to-ferrimagnetic transition. In addition to the geometrical frustration, some rearrangement of Co^{2+} and Co^{3+} ions may play some role in the unusual transition. Further study is necessary to settle the problem.

We now discuss the T dependence of ΔP_c . The change in ΔP_c across T^* is of the order of 0.1 mC/m^2 . In contrast, it reaches 17 mC/m^2 across the ferrimagnetic phase transition [14]. It has been proposed that ΔP_c can be explained by exchange striction [18,19]. ΔP_c is nearly proportional to the average of the scalar product of the magnetic moment S_T on the triangular layer and neighboring moments S_{K_i} ($i = 2, 3, 4$) on the upper and lower kagome layers. ΔP_c in the intermediate-temperature phase should be smaller than that in the ferrimagnetic phase because of the disordered magnetic moments on triangular layers. In contrast, Co tetrahedra should be distorted cooperatively in the ferrimagnetic phase, since the sign of $\sum_i S_T \cdot S_{K_i}$ for adjacent triangular and kagome layers is negative for every column.

In summary, we have carried out a single-crystal neutron diffraction measurement and confirmed that $\text{CaBaCo}_4\text{O}_7$ undergoes an antiferromagnetic transition at T^* . We propose an antiferromagnetic structure between T_C and T^* , where the unit

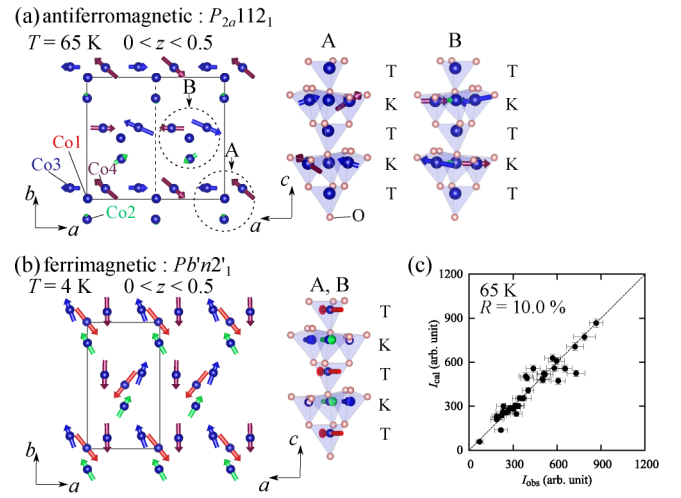


FIG. 3. (a) Possible monoclinic antiferromagnetic structure of $P_{2a}112_1$ at $T = 65 \text{ K}$. Projections onto (left) the c plane for $0 < z < 0.5$ and (right) the b plane. T and K denote layers of the Co triangles and kagome, respectively. (b) Ferrimagnetic structure below T_C suggested in Ref. [13]. Projections onto (left) the c plane for $0 < z < 0.5$ and (right) the b plane. (c) Comparison between I_{obs} and I_{cal} for the magnetic model at 65 K.

cell is doubled along the a axis. The intermediate-temperature phase hosts essentially partial order of Co magnetic moments on the kagome layers. The present study proposes a possibility that the large ME response in $\text{CaBaCo}_4\text{O}_7$ may arise from the large change in exchange striction with the transition between antiferromagnetic and ferrimagnetic phases.

ACKNOWLEDGMENTS

We thank Dr. Matsuura for assistance with the ultrasound velocity measurements. The neutron scattering measurements were performed at the Materials and Life Science Experimental Facility of the J-PARC under User Program No. 2018A0161. The x-ray diffraction experiments were performed with the approval of the Photon Factory Program Advisory Committee (Proposals No. 2015T004, No. 2017G175, and No. 2020R-05). The measurements of the magnetization and Laue photographs were carried out at the Institute for Solid State Physics, The University of Tokyo, Kashiwa, Japan. This work was supported by JSPS KAKENHI Grants No. JP16H01065, No. JP19H05826, and No. 19H01835. T.O. was supported by the Japan Society for the Promotion of Science through the Program for Leading Graduate Schools (MERIT).

- [1] N. A. Spaldin and R. Ramesh, *Nat. Mater.* **18**, 203 (2019).
- [2] S. Manipatruni, D. E. Nikonov, and I. A. Young, *Nat. Phys.* **14**, 338 (2018).
- [3] D. N. Astrov, *Sov. Phys. JETP* **11**, 708 (1960).
- [4] Y. Tokura, S. Seki, and N. Nagaosa, *Rep. Prog. Phys.* **77**, 076501 (2014).

- [5] T. Kimura, T. Goto, H. Shintani, K. Ishizaka, T. Arima, and Y. Tokura, *Nature (London)* **426**, 55 (2003).
- [6] A. H. Arkenbout, T. T. M. Palstra, T. Siegrist, and T. Kimura, *Phys. Rev. B* **74**, 184431 (2006).
- [7] K. Taniguchi, N. Abe, S. Ohtani, and T. Arima, *Phys. Rev. Lett.* **102**, 147201 (2009).

- [8] G. Lawes, A. B. Harris, T. Kimura, N. Rogado, R. J. Cava, A. Aharony, O. Entin-Wohlman, T. Yildirim, M. Kenzelmann, C. Broholm, and A. P. Ramirez, *Phys. Rev. Lett.* **95**, 087205 (2005).
- [9] T. Kimura, J. C. Lashley, and A. P. Ramirez, *Phys. Rev. B* **73**, 220401(R) (2006).
- [10] S. Seki, Y. Yamasaki, Y. Shiomi, S. Iguchi, Y. Onose, and Y. Tokura, *Phys. Rev. B* **75**, 100403(R) (2007).
- [11] A. Apostolov, I. Apostolova, and J. Wesselinowa, *Solid State Commun.* **292**, 11 (2019).
- [12] Z. Qu, L. Ling, L. Zhang, L. Pi, and Y. Zhang, *Solid State Commun.* **151**, 917 (2011).
- [13] V. Caignaert, V. Pralong, V. Hardy, C. Ritter, and B. Raveau, *Phys. Rev. B* **81**, 094417 (2010).
- [14] V. Caignaert, A. Maignan, K. Singh, C. Simon, V. Pralong, B. Raveau, J. F. Mitchell, H. Zheng, A. Huq, and L.C. Chapon, *Phys. Rev. B* **88**, 174403 (2013).
- [15] V. Cuartero, J. Blasco, G. Subas, J. Garca, J. A. Rodriguez-Velamazn, and C. Ritter, *Inorg. Chem.* **57**, 3360 (2018).
- [16] H. Iwamoto, M. Ehara, M. Akaki, and H. Kuwahara, *J. Phys.: Conf. Ser.* **400**, 032031 (2012).
- [17] S. Bordács, V. Kocsis, Y. Tokunaga, U. Nagel, T. Rődm, Y. Takahashi, Y. Taguchi, and Y. Tokura, *Phys. Rev. B* **92**, 214441 (2015).
- [18] R. D. Johnson, K. Cao, F. Giustino, and P. G. Radaelli, *Phys. Rev. B* **90**, 045129 (2014).
- [19] R. S. Fishman, S. Bordács, V. Kocsis, I. Kézsmárki, J. Viirik, U. Nagel, T. Rődm, A. Puri, U. Zeitler, Y. Tokunaga, Y. Taguchi, and Y. Tokura, *Phys. Rev. B* **95**, 024423 (2017).
- [20] S. Yu, C. Dhanasekhar, V. Adyam, S. Deckoff-Jones, M. K. L. Man, J. Madéo, E. L. Wong, T. Harada, M. B. Murali Krishna, K. M. Dani, and D. Talbayev, *Phys. Rev. B* **96**, 094421 (2017).
- [21] T. Sarkar, M. Motin Seikh, V. Pralong, V. Caignaert, and B. Raveau, *Appl. Phys. Lett.* **100**, 232401 (2012).
- [22] C. Dhanasekhar, A. K. Das, R. Singh, A. Das, G. Giovannetti, D. Khomskii, and A. Venimadhav, *Phys. Rev. B* **96**, 134413 (2017).
- [23] M. M. Seikh, V. Caignaert, E. Suard, K. Preethi Meher, A. Maignan, and B. Raveau, *J. Appl. Phys. (Melville, NY)* **116**, 244106 (2014).
- [24] J. Lohr, A. L. Larralde, J. Curiale, R. Sánchez, J. Campo, G. J. Cuello, D. Sheptyakov, L. Keller, M. Kenzelmann, and G. Aurelio, *Phys. Rev. B* **102**, 134406 (2020).
- [25] V. Caignaert, V. Pralong, A. Maignan, and B. Raveau, *Solid State Commun.* **149**, 453 (2009).
- [26] B. Wolf, B. Lüthi, S. Schmidt, H. Schwenk, M. Sieling, S. Zherlitsyn, and I. Kouroudis, *Physica B (Amsterdam)* **294**, 612 (2001).
- [27] T. Ohhara, R. Kiyonagi, K. Oikawa, K. Kaneko, T. Kawasaki, I. Tamura, A. Nakao, T. Hanashima, K. Munakata, T. Moyoshi, T. Kuroda, H. Kimura, T. Sakakura, C.-H. Lee, M. Takahashi, K.-i. Ohshima, T. Kiyotani, Y. Noda, and M. Arai, *J. Appl. Crystallogr.* **49**, 120 (2016).
- [28] S. N. Panja, J. Kumar, S. Dengre, and S. Nair, *J. Phys.: Condens. Matter* **28**, 486001 (2016).
- [29] B. Raveau, V. Caignaert, V. Pralong, and A. Maignan, *Z. Anorg. Allg. Chem.* **635**, 1869 (2009).
- [30] K. Momma and F. Izumi, *J. Appl. Crystallogr.* **44**, 1272 (2011).
- [31] Y.-W. Cui, T. Koyama, I. Ohnuma, K. Oikawa, R. Kainuma, and K. Ishida, *Acta Mater.* **55**, 233 (2007).
- [32] We also considered the domain ratio of another twin caused by orthorhombic-to-monoclinic transition for each model, and the twin volume fraction turned out to be nearly 1.
- [33] J. C. Lashley, R. Stevens, M. K. Crawford, J. Boerio-Goates, B. F. Woodfield, Y. Qiu, J. W. Lynn, P. A. Goddard, and R. A. Fisher, *Phys. Rev. B* **78**, 104406 (2008).
- [34] M. Matsuda, J.-H. Chung, S. Park, T. J. Sato, K. Matsuno, H. A. Katori, H. Takagi, K. Kakurai, K. Kamazawa, Y. Tsunoda, I. Kagomiya, C. L. Henley, and S.-H. Lee, *EPL* **82**, 37006 (2008).